UNIVERSITY OF OKLAHOMA

GRADUATE COLLEGE

DETECTABILITY ASSESSMENT OF THE HIGH-ENERGY X-RAY IN-LINE PHASE CONTRAST PROTOTYPE FOR DENSE BREASTS

A THESIS

SUBMITTED TO THE GRADUATE FACULTY

in partial fulfillment of the requirements for the

Degree of

MASTER OF SCIENCE

By

YURAN GUO
Norman, Oklahoma
2018

DETECTABILITY ASSESSMENT OF THE HIGH-ENERGY X-RAY IN-LINE PHASE CONTRAST PROTOTYPE FOR DENSE BREASTS

A THESIS APPROVED FOR THE
SCHOOL OF ELECTRICAL AND COMPUTER ENGINEERING

BY

Dr. Hong Liu, Chair

Dr. Yuchen Qiu

Dr. Bin Zheng

This thesis is dedicated to my parents and my grandmother, who support me and give me endless love during my study. Words cannot express my gratitude for being blessed with them.

Acknowledgements

It is of my great honor to be allowed as a member in Dr. Liu's lab. The guidance I received from Dr. Liu is extremely precious. He is a patient and experienced professor and the knowledge he taught to me is of great importance for my future development. I would like to express my gratitude for his help and guidance during my master's study.

I would also like to appreciate the help and patience from the other member in my lab: Dr. Yuhua Li, Dr. Di Wu, Farid H. Omoumi, Dr. Muhammad U. Ghani, and Dr. Molly D. Wong. I am grateful for their help whenever I was stuck on the problems. Also, I am especially grateful for the advices and suggestions given by Dr. Molly D. Wong and Dr. Muhammad U. Ghani on my thesis. Without their patience and assistance, it would be more difficult for me to finish my study.

Finally, I would like to express my gratitude to the other members from my committee, Dr. Bin Zheng and Dr. Yuchen Qiu, for their help during the time on my thesis.

Table of Contents

List of Tables

List of Figures

Abstract

The primary objective of the research in this thesis is to evaluate the performance of the high-energy in-line phase contrast prototype with the conventional mammography along with ultrasound systems in the detection of tumors within dense breasts. Mammography is the gold standard for breast cancer screening. The accuracy of conventional mammography decreases in imaging of dense breasts. Additional screening with supplemental modality, such as ultrasound, increases the rate of early detection of breast cancer in women with dense breasts. However, the ultrasound also has the disadvantages of operator dependent, high false-positive rate, etc. Therefore, there is room for the improvement in mammography particularly in dense breast imaging. Phase contrast x-ray imaging provides a unique opportunity in improving the accuracy of cancer detection in breast imaging. Phase contrast imaging relies not only on the attenuation coefficients but also on the effects produced by x-ray phase shift coefficients. In this study, three breast phantoms are used for imaging comparisons. The first phantom containing simulated tumors is commercially manufactured in 50-50 glandular-adipose ratio (50G-50A). Two phantoms in 70-30 glandular-adipose ratio (70G-30A) are custom made with one phantom embedded with gelatin blocks and the other phantom embedded with carbon fiber disks to simulate various tumor sizes. The phase contrast images are acquired with optimized operating parameters. With the preliminary study of 50G-50A phantom, the results indicate that the conventional technique is not able to detect the tumor-like object while the ultrasound and the in-line phase contrast prototype are able to detect the object in the phantom, under the specific experimental condition. For both the 70G-30A phantoms, conventional technique did not

detect any objects, ultrasound detected all the objects while the phase contrast imaging detected more than 60% of the embedded tumor-like objects. The results of the research in this thesis demonstrate that the high-energy in-line phase contrast imaging has the potential to be a standalone modality in screening of breast cancer.

Chapter 1. Introduction

1.1 Significance

Breast cancer is one of the most prevalent type of cancer in women, accounting for more than one fourth of all diagnosed cancers in women [1]. One of the strategies to reduce breast cancer mortality is early detection, as it is more easily treated at early than advanced stages. Screening mammography has been the most accepted breast cancer detection tool for several decades, and numerous clinical studies have proven its key role in the reduction of breast cancer mortality [2-7]. However, when imaging dense breasts, screening mammography has lower performance because of its limited sensitivity to the breast tumors [3, 8-11]. This phenomenon can be explained by the principle of conventional x-ray mammography, which is based on the attenuation effect of x-ray beam. When x-ray waves pass through the human breast, they interact with the body tissues and attenuated. The amount of attenuation varies based on the type of tissue. The human breast consists mostly of fat, epithelium and connective tissue. Radiology studies have demonstrated that the fat (also known as adipose) tissue is radiographically lucent, which means that it has a small attenuation coefficient. However, the other breast tissues, such as fibrous and glandular tissues, are radiographically dense, meaning that they have higher attenuation coefficients [4-6, 8, 10]. However, the attenuation coefficients of glandular tissue are very close to the attenuation coefficients of malignant breast tissue [12]. Therefore, it is challenging to distinguish malignant breast tissue from normal breast tissue, and this challenge increases when imaging breasts with high glandular composition. Also, since the glandular tissue is related with the breast density, in the clinical applications, the breast

density is used as an indicator of the human breast glandular composition. A dense breast usually indicates to a breast with high glandular composition. The American College of Radiology (ACR) has categorize the breast density into four different level: almost entirely fatty (category A), scattered areas of fibroglandular density (category B), heterogeneously dense (category C) or extremely dense breast (category D). Investigation have shown that about 43%-55% women who aged 40 to 74 years old in the United States have dense breasts where the majority of these are classified as category C [13]. Some studies have also indicated that women with higher breast density have a higher risk of developing breast cancer in their lifetime [14-16]. Thus it is critical to provide the ability to effectively distinguish between benign and malignant breast tissue in dense breasts during the breast cancer screening process.

In order to improve the limited efficacy of mammography, ultrasound is typically used as supplementary equipment in current clinical breast screening. Data shows that when ultrasound is utilized in breast cancer screening, the detection accuracy is increased compared with using screening mammography alone [13, 17, 18]. Although this combination does improve breast cancer detection, ultrasound also suffers from the challenges of high operator dependence and variable image quality [10]. Also, many suspicious tissues found by ultrasound are proven not to be malignant breast tumor by biopsy [17, 18]. Thus, a new imaging modality is still needed to significantly increase the accuracy of detecting breast cancer, in particular for dense breasts as compared to conventional mammography and ultrasound imaging modalities.

1.2 Specific Aims

An emerging technology called in-line phase contrast imaging has the potential ability to improve the accuracy of breast cancer detection. In the geometry of the in-line phase contrast prototype system, there is a specific distance between the object and the detector, which is called the air gap. The air gap brings two advantages to in-line phase contrast imaging: (1) reduction of scattered photons, and (2) a propagation distance for the phase shift differences from various human tissues to interfere, which produces edge enhancements on the image [19-24]. Similar to attenuation, phase shifts are a property of electromagnetic waves and occur at varying amounts when passing through objects, depending on the refraction index of the imaged object. The difference in refraction indices between benign and malignant tissue is much higher than the difference in attenuation indices; therefore, enhanced image contrast is provided by phase contrast imaging in comparison to conventional imaging [25]. In addition, the in-line phase contrast technique combines the phase shift effects along with the attenuation effects, which results in enhanced image contrast that provides the ability to distinguish malignant tissue from benign breast tissue.

In-line phase contrast imaging has attracted significant research attention in the field of clinical applications over the last two decades, especially for breast imaging. First, it has been validated that the phase contrast technique can increase the image quality compared with the conventional x-ray technique [20-23, 26, 27]. Secondly, it has also been validated that the phase contrast technique has the potential to reduce the radiation dose to the patients [20, 27-31]. At the same time, the potential of the in-line phase contrast tomosynthesis prototype [32-36] as well as the potential of the low-energy in-line phase

contrast x-ray mammography prototype in breast cancer detection have also been proven by numerous studies [37, 38]. Furthermore, several studies have demonstrated that increasing the x-ray energy has the potential to further decrease the radiation dose to the patients [39-41]. Finally, the potential of using high-energy in-line phase contrast for the detection of breast cancer in normal density breast tissues has also been illustrated [42, 43]. However, there are few studies focused on the detection of high-density breast tissue using high energy phase contrast imaging.

The primary objective of the research in this thesis is to evaluate the performance of the high-energy in-line phase contrast prototype as compared with the conventional mammography along with the ultrasound systems in the detection of tumors, particularly within dense breast tissues. Three breast phantoms were used for imaging comparisons. The first phantom embedded with simulated tumors is commercially manufactured in 50-50 glandular-adipose ratio. A preliminary study is conducted by using this breast phantom to investigate the performance of the imaging modalities in the breast with normal density. Two lab-made phantoms, which mimic 70-30 glandular-adipose ratios, are also used in this study to evaluate the performance of the imaging modalities for dense breasts. These two 70-30 breast phantoms are embedded with gelatin blocks and carbon fiber disks with various tumor sizes, respectively. These studies consist of comparisons between images of breast phantoms taken by the conventional x-ray system together with screening ultrasonography and the high-energy in-line phase contrast prototype system alone. In order to be more specifically evaluate the performance of the high energy in-line phase contrast x-ray imaging prototype. An observer performance study is also conducted to

compare the performance of the conventional x-ray imaging and the high energy in-line phase contrast imaging in the detection of the objects in 70-30 breast phantoms.

1.3 Organization of Thesis

The organization of this thesis is as follows: First, Chapter 2 presents the theory of conventional x-ray imaging and the ultrasound imaging, and the background of their application in the breast cancer screening. Second, Chapter 3 introduces the theory of phase contrast imaging, its supporting technology and its advantages. Then Chapter 4 presents the description of the imaging systems used in this study. Next, Chapter 5 introduces the breast phantoms employed in this study. After that, Chapter 6 reveals the results of the experiments, giving a comprehensive comparison between traditional breast screening method (the conventional mammography together with the screening ultrasound) with using the high-energy in-line phase contrast prototype system alone. Finally, Chapter 7 summarizes and analyses the results of the research presented in this thesis, discusses the remained challenges and the corresponding research direction in the future.

Chapter 2. Background and Theory of the Conventional X-ray Imaging and Ultrasound Imaging

The mammography along with the supplemental ultrasound is applied in the current breast cancer screening in dense breasts. Also, the technique of current mammography equipment is based on the principle of the conventional x-ray imaging. In this chapter, we are going to introduce the principle of the conventional x-ray imaging and the ultrasound imaging.

2.1 Conventional X-ray Imaging

In current clinical applications, x-ray photons are generated through the energy conversion of the electrons. As shown in the Figure 2-1 below, in a bremsstrahlung spectrum x-ray tube, all the components of the x-ray tube are set in an evacuated envelop.

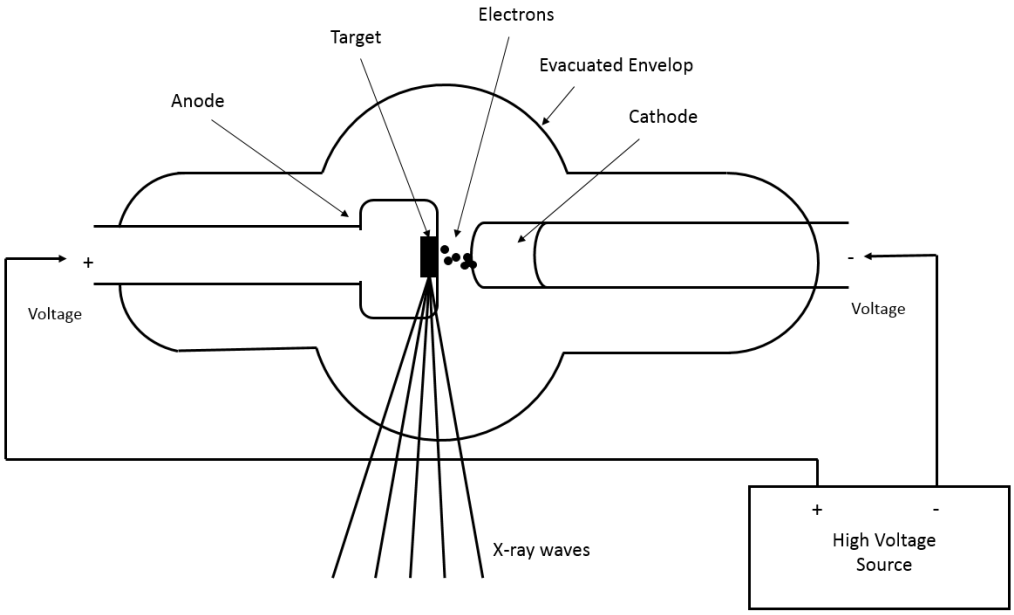

Figure 2-1: Illustration of the concept of x-ray tube

When an electric potential difference is applied between the cathode and the anode, the negative charged electrons at the cathode will be attracted and travel to the positive charged anode area. The electrons are accelerated during this process because of the applied electric potential difference, resulting in an increasing kinetic energy of the electrons. When the electrons arrive the anode, it impacts with the target on the anode and the kinetic energy is converted to the other form of energy, mostly is the unwanted heat. However, when the electrons come close to the positive charged nucleus in the target, the coulombic force between the electron and the nucleus will decrease the speed of the electrons. Thus, the kinetic energy of the electrons is decreased and those energy is converted to the energy of the x-ray photons.

When the x-ray beam is generated from the x-ray tube, it will pass through the human body. There are three main interactions between the x-ray and human body during this process: (1) Rayleigh scattering, (b) Compton Scattering, and (c) Photoelectric effect [44].

The Rayleigh scattering (Figure 2-2) mainly occurs when the x-ray photon interacts with the soft tissue [44]. In Rayleigh scattering, the incident x-ray photon (λ_1) is interacting with the entire atom. During this interaction, a scattered photon (λ_2) with the same photon energy but different direction as the incident x-ray photon will then be emitted from the atom. Once they are received by the x-ray detector, they will be converted to the image signal. In mammography imaging system, the scattered photon carries useless information and can degrade image quality when it is detected by the detector. Thus, the x-ray image system is required to avoid the number of scatter photons as much as possible. Luckily, the probability of the occurrence of Rayleigh scattering is relatively small, with the probability

of 5% at the photon energy greater than 70 keV and with the probability of 12% at the photon energy of about 30 keV [44].

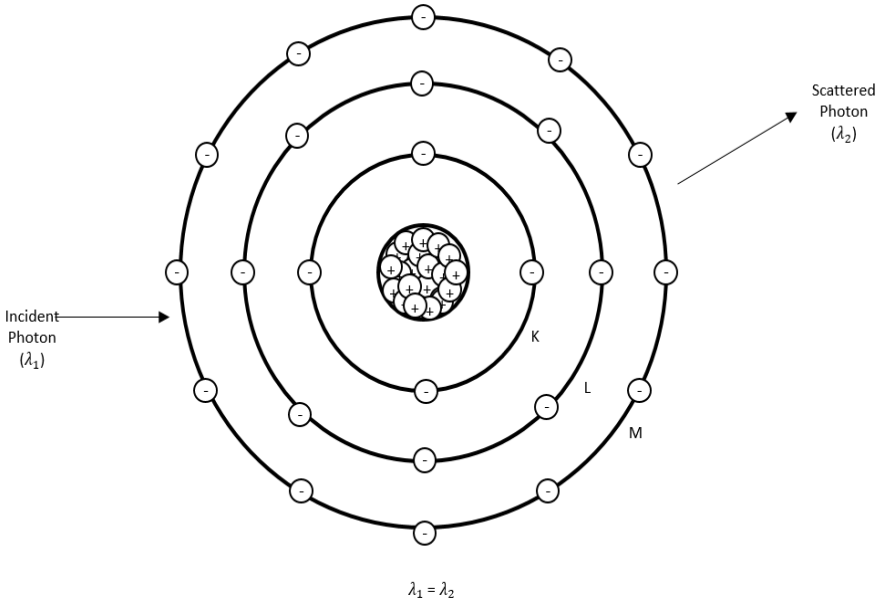

Figure 2-2: Illustration of the concept of rayleigh scattering

The Compton scattering (Figure 2-3) is the primary interaction of x-ray in the clinical applications. In Compton scattering, the incident x-ray photons (λ_1) mainly interact with the outer shell electrons in atoms, instead of the entire atoms. An energy conversion happens during this interaction, results in a scattered photon (λ_2) with the kinetic energy of E_s and an electron (E_e-) emitted from the atom. The relationship between the energy of the incident photon (E_0) and the energy of the scatter photon (E_s) along with the ejected electron (E_e-) is given by the following equation [44]:

$$E_0 = E_s + E_e\text{-} \tag{1}$$

In this equation, the binding energy of the electron in the atom is relatively small and is ignored.

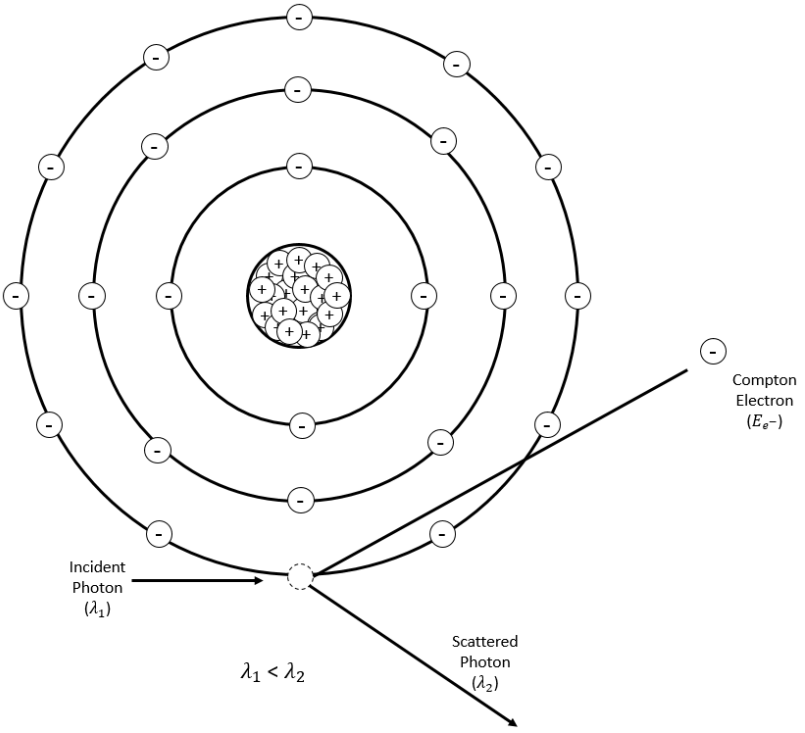

Figure 2-3: Illustration of the concept of compton scattering

Notice that, the energy of the scattered photon can is given by [44]:

$$E_s = \frac{E_0}{1+\frac{E_0}{511\,keV}(1-\cos\theta)} \tag{2}$$

where E_s represents the energy of the scattered photon, E_0 represents the energy of the incident photon and θ represents the angle of the scattered photon. One can see that, for a given angle, the energy of the scattered photon is dependent on the energy of the incident photon. Furthermore, in order to let the electron be ejected from the atom, the energy of the incident photon must be higher than the electron's binding energy. Therefore, the probability of the Compton Scattering will be increased in the x-ray photons with higher energy level.

In the photoelectric effect, the incident photon will also interact with the electrons and be absorbed. According to the energy conservation law, the kinetic energy of the ejected electron (E_{e^-}) is equal to the difference between the energy of the incident photon (E_0) and the binding energy (E_b). As shown in the equation [44]:

$$E_{e^-} = E_0 - E_b \tag{3}$$

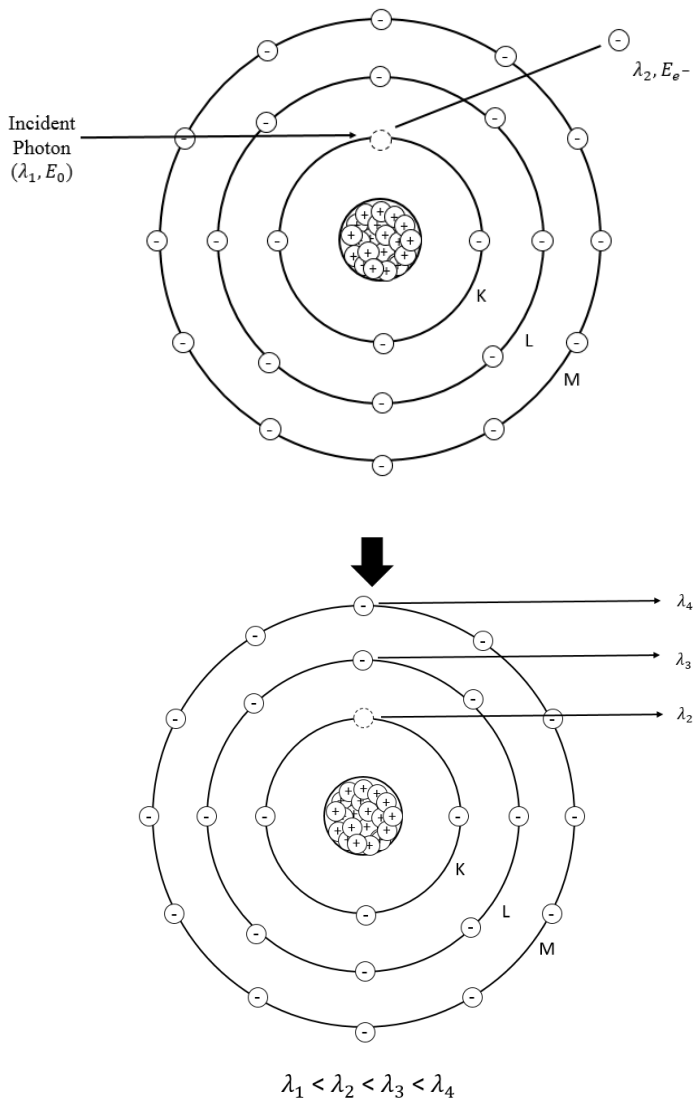

Figure 2-4: Illustration of the concept of photoelectric effect

In order to let the electron to be emitted from the atom, the photoelectric effect happens when the energy of the incident photon is slightly higher than the binding energy of the electrons. As shown in the Figure 2-4 above, the photoelectric effect happens between the incident photon (λ_1) with the energy of E_0 and an electron in the K-shell. The electron will be ionized and ejected with the kinetic energy of E_e- (λ_2). Since this happens at the inner shell of an atom, an electron from the lower binding energy shell will fill this vacancy and

emit another photon (λ_3). The energy of this photon equals to the energy difference between the binding energy of the two shells. This process will cause another vacancy and it will be filled by an electron from the outer binding energy shell and eject another photon (λ_4). Thus, photoelectric effect would cause an electron cascade from the lower binding energy shells to the higher binding energy shells.

The probability of the photoelectric absorption is proportionally dependent on the ratio of $\frac{Z^3}{E^3}$ [44], where Z is the atomic number of the atom and E is the energy of the incident x-ray photons. One can see that the probability of the photoelectric effect is highly energy dependent, for example, the probability of the photoelectric effect of the photons with the energy of 25 keV is $(\frac{100}{25})^3 = 64$ times lower than the probability of the photons with the energy of 100 keV. Thus, the probability of the occurrence of photoelectric effect is much higher in the low energy x-ray photons.

As mentioned previously, when an x-ray wave passing through the human body it will interact with the human body mainly through three ways: the Rayleigh scattering, the Compton Scattering, and the Photoelectric effect. All of these interactions cause the x-ray attenuation. The linear attenuation coefficient μ is used to quantitatively describe the fraction of photons attenuated from the x-ray beams by the materials [44]:

$$\mu \approx \mu_{Rayleigh} + \mu_{Compton} + \mu_{photolectric} \tag{4}$$

where $\mu_{Rayleigh}$, $\mu_{Compton}$ and $\mu_{photolectric}$ represents the attenuation coefficient of the Rayleigh Scattering, the Compton Scattering, and the Photoelectric effect, respectively.

The contribution of these interactions are varied depending on different x-ray beam quality and material conditions.

When an x-ray beam is transmitted through a thick or thin a slab of material with the thickness of x cm, an exponential relationship between the number of input x-ray photons N_0 and output photons N can be expressed by the following equation [44]:

$$N = N_0 e^{-\mu x} \tag{5}$$

where μ represents the linear attenuation coefficient. One may notice that the thickness of the object is also an important factor to attenuate the x-ray beams. Thus, during the clinical mammography detection, human breasts are compressed in order to decrease the attenuation effect caused by the object thickness.

From equation 5, we can see that if two adjacent objects have a big difference in the attenuation coefficient, the contrast of the x-ray image would be higher. However, studies have shown that the attenuation coefficients of the breast tumor tissues and the glandular tissues are very close [12]. As mentioned in Chapter 1, breasts with high glandular composition indicates to a higher density. Therefore, it would be more difficult for the mammography to detect the breast tumors within dense breasts. Investigation have shown that the sensitivity of mammography for normal dense breasts is 75%-90%, however, it drops to 30%-48% for the dense breasts [45, 46]. Therefore, a supplemental equipment is used in the current dense breast screening.

2.2 Ultrasound Imaging

In the current clinical applications, the ultrasound is used as a supplemental equipment in the detection of breast tumors within dense breasts. In this section, we are going to introduce the principle of the ultrasound imaging system, the investigation data of applying the ultrasound in the breast cancer screening, the advantages and disadvantages of using the ultrasound in the breast cancer screening.

2.2.1 Principle of Ultrasound Imaging

The ultrasound waves are generated from the transducer. Once the ultrasound waves are generated, it will propagate through human body. As shown in Figure 2-5, once the ultrasound waves reach the boundary of two different objects, some of the ultrasound waves will be reflected back and some of the ultrasound waves will continue transmitting through the human body.

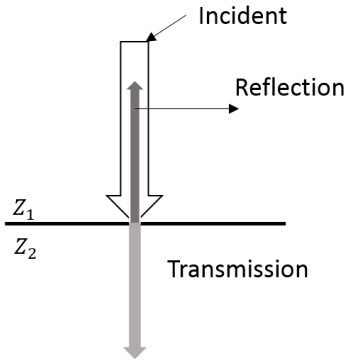

Figure 2-5: Illustration of the concept of the reflection of the ultrasound wave

The magnitude of the reflection is represented by the intensity reflection coefficient, R_I [44]:

$$R_I = \frac{I_r}{I_i} = \left(\frac{Z_2 - Z_1}{Z_2 + Z_1}\right)^2 \quad (6)$$

The Z is called acoustic impedance, which is defined as $Z = \rho c$, where ρ is the density of the material and c is the speed of sound propagate in the medium. One can see that the reflection coefficient is determined by the difference between the properties of the two mediums. The ultrasound image is generated after the reflected ultrasound wave is received by the transducer.

2.2.2 Dense Breast Screening with the Ultrasound

Studies have also demonstrates an increased sensitivity of using the ultrasound as the supplemental screening equipment in the breast cancer detection. Kelly et al has demonstrated that among 6425 studies, 23 breast cancer cases are diagnosed by mammography alone, while 46 breast cancer cases are diagnosed when the breast ultrasound is used as a supplemental diagnostic equipment. Furthermore, the sensitivity of the screening results increased from 40% to 81% after the breast ultrasound is deployed in the breast screening [47]. Also, from Benson et al, among 537 patients with the breast cancer symptomatic, the ultrasound screening is positive in 497 patients, while the mammography is positive in 467 patients [48]. Furthermore, Berg et al also demonstrates that among 4841 patients with dense breast conditions, the sensitive of using the mammography alone is 0.52 while the sensitive of the mammography plus ultrasound is 0.84 [49]. From, the above studies, one can see that the supplemental ultrasound did increase the accuracy of the breast cancer screening.

2.2.3 Disadvantages of the Ultrasound

There are still several disadvantages for the ultrasound to be used as the supplemental equipment in the breast cancer screening. Firstly, even though the ultrasound did increase the accuracy of the breast cancer screening, the recall rate of the ultrasound is still higher than the mammography. Some of the reported tumors by ultrasound shows negative results from biopsy [50]. Also, during the screening, the doctors need to hold the transducer and move through the whole breast to find the breast tumors. Therefore, it is unavoidable that the breast tumor would be missed because of the complicated operation procedure compared with the mammography, especially with the breasts with bigger sizes. Furthermore, since two imaging modalities are used in the breast cancer screening for dense breasts, it will results in a higher time consumption and a higher psychology stress to the patients compared with using single modality. All in all, there is still a room to improve the current breast screening method.

Chapter 3. Phase Contrast X-ray Imaging

3.1 Background and Theory of Phase Contrast X-ray Imaging

As mentioned previously, the principle of conventional x-ray imaging is based solely on the attenuation experienced by the x-ray beam as it passes through an object. The x-ray photons are absorbed in varying amounts corresponding to the biological properties of the structures within the object, which produces differences in contrast on an x-ray image [44]. The difference in biological composition between bones and soft tissue produces very high contrast between them, but the very similar composition between benign and malignant tissue results in low contrast, which renders it difficult to distinguish between them on a conventional x-ray image [26, 27]. However, the emerging technology of phase contrast imaging has the potential to overcome this challenge. Phase contrast imaging is based on the definition of an x-ray as an electromagnetic wave, which means it will also experience phase changes as it passes through an object [19, 23]. Contrast is produced on a phase contrast image based on both the attenuation effects and the refraction effects, which also vary based on the different biological properties of the structures within the object. The amount of the phase change is determined by the refractive index n, which can be represented as a complex formula [23]:

$$n = 1 - \delta + i\beta \tag{7}$$

where δ is the real part of n, which is responsible for the x-ray phase shift (ϕ), and β is the complex part of n, which is responsible for the x-ray absorption.

The value of δ is given as [23]:

$$\delta = \left(\frac{r_e \lambda^2}{2\pi}\right) \sum_l N_l (Z_l + f_l^r) \tag{8}$$

where λ, r_e, Z_l, f_l^r, N_l are the wavelengths of the x-ray beams, classical electron radius, atomic number of element l in the object, the real part of the anomalous scattering factor, atomic density, respectively.

The value of β is given by the following formula [23]:

$$\beta = \left(\frac{r_e \lambda^2}{2\pi}\right) \sum_l \left(N_l f_l^i\right) \tag{9}$$

where f_l^i is the imaginary part of the anomalous scattering factor.

In a three-dimensional situation, the corresponding phase shift φ and linear attenuation coefficient μ are given by [23]:

$$\varphi(x, y) = \frac{2\pi}{\lambda} \int \delta(x, y, z) dz \tag{10}$$

$$\mu(x, y) = \frac{4\pi}{\lambda} \int \beta(x, y, z) dz \tag{11}$$

Theoretical calculations demonstrate that the x-ray phase shift factor is much bigger than the x-ray attenuation factor for a given type of tissue [23]. Therefore, since phase contrast imaging combines both attenuation and refraction effects to produce contrast on the x-ray image, it has the potential to greatly improve the image quality as compared to conventional mammography.

3.2 Phase Contrast X-ray Imaging Techniques

Currently, there are five different techniques developed for the phase contrast imaging: the X-ray Interferometry [19], the Diffraction-Enhanced Imaging (DEI) [51], In-line Phase Contrast Imaging [21, 23], Grating Based Phase Contrast Imaging [52] and Speckle Based Phase Contrast Imaging [53]. The X-ray Interferometry, DEI, and the In-line Phase Contrast Imaging will be presented in detail in the following sections.

3.2.1 X-ray Interferometry

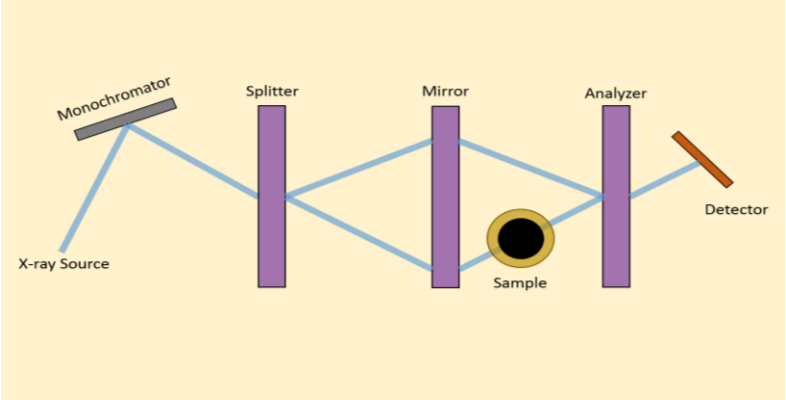

Figure 3-1: Illustration of the concept of x-ray interferometry technique

The x-ray interferometry is the earliest technique used in the phase contrast x-ray imaging. It consists of three perfectly matched beam crystals and one beam filter [19]. As shown in Figure 3-1. The incident x-ray beam is firstly filtered by the monochromator and then reflected to the first crystal (splitter). When the monochromatic beam arrives at the first crystal, it is divided into two beams: one beam remains unchanged, which is regarded as the reference beam, while the other beam interacts with the sample. When the two beams arrives at the second crystal (mirror), their propagation direction are changed. The sample is placed between the second and the third crystal. When one of the two beams passing

through the object, it experiences phase change (ϕ). The two beams converge at the third crystal (analyzer) and an interference pattern is then generated depending on the phase difference of the two beams. This pattern is finally detected by the detector.

Momose et al used this technique to image the rat cerebellum and rabbit cancer lesions with the x-ray interferometry CT [54]. The advantage of X-ray interferometry is that it is more sensitive to the subtle change of the phase shift. However, the crystal alignment and stability is required on the order of 0.01 nm, which is hard to be applied in the current clinical applications.

3.2.2 Diffraction-Enhanced Imaging (DEI)

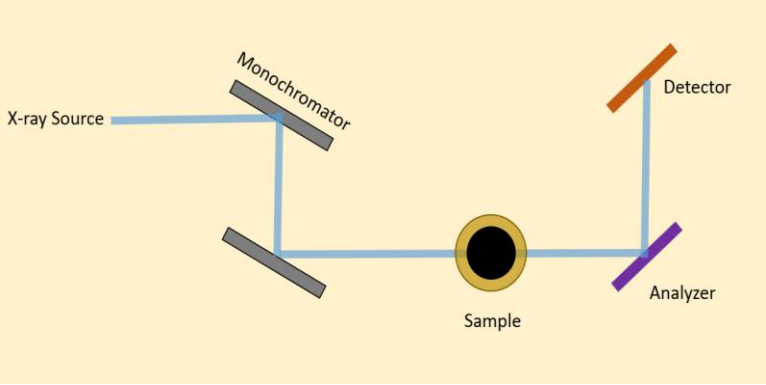

Figure 3-2: Illustration of the concept of diffraction-enhanced imaging technique

The second technique to be introduced is called diffracted-enhanced imaging (DEI). The DEI system consists of an x-ray source, a monochromator, an analyzer, and a detector. As shown in the Figure 3-2, the x-ray wave passes through a paralleled monochromator. Only the wavelength who meets the Bragg Equation [51]:

$$2d\sin(\theta \pm \Delta\theta) = \lambda \pm \Delta\lambda \tag{12}$$

can be reflected by the monochromator. When the monochromatic x-ray beams pass through the sample, it is reflected by the analyzer to the detector. The analyzer is also used as a monochromator to reflect the light beams which carry useful information and to vanish the scattered photons which does not meet the requirement of Bragg Equation. Finally, a clear phase contrast x-ray image appears on the x-ray detector thanks to the filtered x-ray photons by the analyzer.

D. Champan used this technique and demonstrated its superior image to the conventional x-ray imaging by using ACR (American College of Radiology) phantom [51]. However, the incident window of the analyzer is very narrow, which means the angle of the analyzer must be placed exactly same as the angle of the monochromator. Therefore, the DEI technique is still very difficult to be realized in the real clinical applications because of its strict equipment component setting requirement.

3.2.3 In-line Phase Contrast Imaging

As discussed previously, the techniques of x-ray interferometry and DEI have both demonstrated their abilities to improve the image quality compared with the conventional x-ray imaging. However, both of the techniques require monochromatic x-ray beams that are currently only available at synchrotron facilities. This presents a major challenge in translating both techniques into clinical applications. Fortunately, the in-line phase contrast x-ray imaging has the potential to overcome the difficulties, as it utilizes polychromatic x-rays from a microfocus tube, both of which are readily available and clinically acceptable [21-23]. In addition, in-line phase contrast imaging utilizes a similar configuration to conventional imaging, which the addition of an air gap between the object and the

detector.The basic principle of the in-line phase contrast x-ray imaging is shown in Figure 3-3 below:

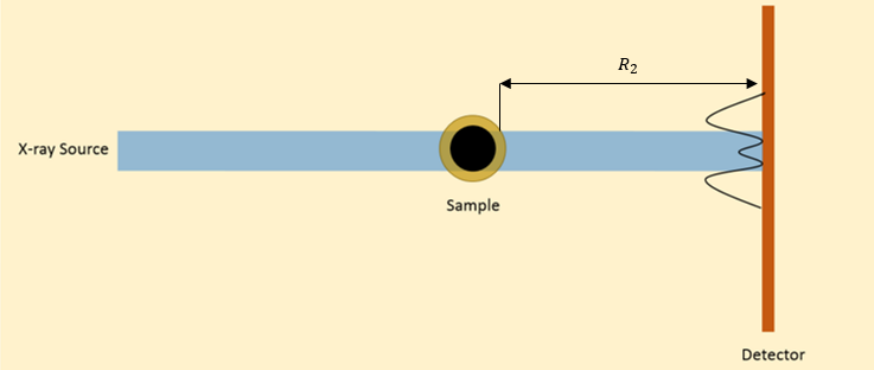

Figure 3-3: Illustration of the concept of in-line phase contrast imaging technique

As with conventional imaging, the x-ray wave-front experiences attenuation as it passes through the object. However, it also experiences refraction, and the distance between the object and the detector in the phase contrast configuration produces an interference pattern on the output image from the phase shift differences between the different structures within the object. The image intensity of the in-line phase contrast imaging technique is given by Equation 13 [23]:

$$I\,(\vec{r}) = \frac{I_{10}}{M^2}\left\{A^2(\vec{r}) - \frac{\lambda R_2}{2\pi M}\left(\nabla^2\left(A^2(\vec{r})\phi(\vec{r})\right)\right)\right\} \tag{13}$$

where λ is the x-ray wavelength, I_{10} is the entrance intensity of the x-ray wave at the object plane, R_2 is the object-to-detector distance, M is the magnification factor, $A^2(\vec{r})$ is the image intensity of the attenuation based image, $\phi(\vec{r})$ is the phase shift of the x-ray wave. From this equation, we can see that the image contrast is proportional to the Laplacian of the phase shift of the x-ray wave. Also, since the phase shift ϕ is proportional to the

refraction index, it follows then that the image intensity of the in-line phase contrast imaging is proportional to the Laplacian of the refraction index of the object.

Even though a monochromatic x-ray source is not required in the in-line phase contrast imaging, there are still several considerations that must be taken in order to implement the in-line phase contrast imaging into clinical applications. The principle of in-line phase contrast requires a very strict spatial coherence condition. From the traditional optical principle, the lateral coherence length $L_{\perp}$ of a monochromatic beam can be described by the formula [56]:

$$L_{\perp} = \frac{\lambda R_1}{s}, \tag{14}$$

where R_1 represents the source-to-object distance and s represents the size of the x-ray source focal spot. In real clinical applications, the coherence length, L_{coh}, should be large enough for phase-contrast visibility. For example, if an x-ray wave with the photon energy of 28 keV is applied from the focal spot size of 50 μm, and with source-to-object distance (SOD) of 1.0 m, one can only reach the lateral coherence length of 0.886 μm. One needs an extremely large distance of 60 m to get a lateral coherence length of 53.16 μm, which is not applicable in the clinical applications. Fortunately, in in-line phase contrast prototype system, the diffraction effect of the x-ray from the object to the detector is another factor that needs to be considered. This effect can be explained by a parameter called phase-space shearing L_{Shear} [56, 59]:

$$L_{Shear} = \frac{\lambda R_2 |u|}{M}, \tag{15}$$

where once again λ is the x-ray wavelength, R_2 represents the object-to-detector distance, u represents the spatial frequency of the object, and M represents the magnification of the prototype system. The coherence effects of phase-contrast visibility can be noted by [56]:

$$\frac{L_{Shear}}{L_{\perp}} = \frac{(M-1)s|u|}{M}, \tag{16}$$

recalling that s represents the size of the x-ray source focal spot. For the case where $\frac{L_{Shear}}{L_{\perp}} << 1$, the x-ray wave is fully coherent over the shearing length and the visibility of phase contrast associated with the structural component is observable under optimized settings. For the intermediate case where $\frac{L_{Shear}}{L_{\perp}} < 1$, the x-ray wave is partially coherent over the shearing length and the phase contrast is partially observable. If $\frac{L_{Shear}}{L_{\perp}} > 1$, the x-ray wave is incoherent over the shearing length and the phase contrast associated with the structural component is not distinguishable.

3.2.4 Image Quality Improvement of In-line Phase Contrast Imaging

Section 3.2.3 introduced the theory of in-line phase contrast imaging. Previous studies have shown that the in-line phase contrast technique has the advantage of image quality improvement as compared with conventional x-ray imaging [32, 33, 37, 40, 43]. This improvement can be attributed to the following factors: edge enhancement effect, geometry magnification, and scattered photons reduction. These factors are introduced in this section.

3.2.4.1 Edge Enhancement Effect

First, phase contrast imaging produces an edge enhancement effect, which provides improved image quality. As mentioned previously, the phase shift shows more contributions on the boundaries between different objects. If we only consider the effect of the x-ray phase shift, the relationship between the image intensity $I(x,y)$ and the phase shift $\emptyset\left(\frac{x}{M},\frac{y}{M}\right)$ can be illustrated by the following equation [23]:

$$I(x,y)=\frac{I_{10}}{M^2}\left\{1-\frac{\lambda R_2}{2\pi M}\nabla^2\left[\emptyset\left(\frac{x}{M},\frac{y}{M}\right)\right]\right\} \tag{17}$$

We can see that the intensity of the x-ray image is related to the Laplacian of the phase shift $\emptyset\left(\frac{x}{M},\frac{y}{M}\right)$. Since the $\emptyset$ is determined by the property of materials, the image intensity will be greatly enhanced on the boundaries between different human tissues.

3.2.4.2 Magnification

Another factor that can improve the image quality of the in-line phase contrast imaging is the magnification. The magnification factor (M) of the object in the image can be calculated by:

$$M=\frac{R1+R2}{R1} \tag{18}$$

The image magnification can increase the Nyquist frequency, thus, results in an improvement of the spatial resolution. This method is also used in the conventional mammography in order to improve the image quality. However, the magnification effect in the conventional x-ray system is limited by the geometry unsharpness, which is also known as penumbra effect. The penumbra effect happens because the ideal point x-ray

source is not available in the realistic applications. Figure 3-4 demonstrate the principle of the penumbra effect. The width of the penumbra effect P is given by [44]:

$$P = F\frac{H-h}{h} \tag{19}$$

where F represents the focal spot size, H represents the source-to-image distance, and h represents the source-to-object distance. However, in the in-line phase contrast imaging, the required small focal size of the x-ray source and the bigger object-to-image-distance can reduce the penumbra effect.

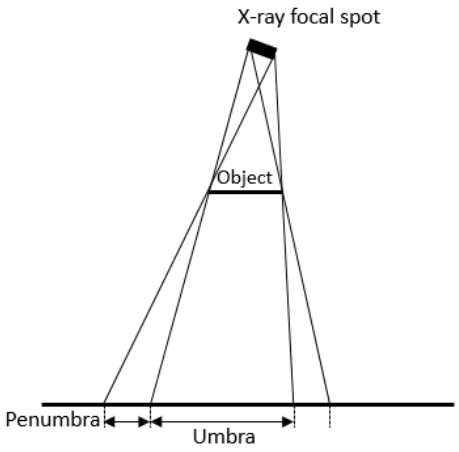

Figure 3-4: Illustration of the concept of penumbra effect

It is hypothesized that the magnification effect together with the benefit of edge enhancement of the in-line phase contrast imaging can possibly offset the edge blurring caused by the penumbra effect. Thus, the influence of the penumbra effect in the in-line phase contrast imaging technique may be reduced compared with the conventional x-ray imaging.

3.2.4.3 Scattered Photons Reduction

In the in-line phase contrast imaging, the introduction of the air gap between the object and the detector can reduce the probability of the scattered x-ray photons detected by the detector, thus, reduce the number of scattered photons received by the detector and results in a higher image quality.

3.2.5 In-line Phase Contrast Imaging with High-energy X-ray Photons

The conventional x-ray breast imaging system requires x-ray photon energy in a relative lower range because an x-ray photon with lower energy have higher probability to produce soft tissue contrast compared with a higher energy x-ray photon. However, the in-line phase contrast x-ray imaging is not only based on the attenuation effect of the x-ray photons but also based on the phase shift effect when the x-ray beams passing through the breast. Theoretical studies have indicated that the decrease of the phase shift factor is less than the decrease of the attenuation factor as the x-ray photon energy increases: in the diagnostic x-ray energy level, the change of phase factor, δ, is proportional to E^{-2} while the change of attenuation factor, β, is proportional to E^{-4} [23, 59], where E represents the energy of the x-ray photons.

As mentioned in Section 3.2.3, in order to meet the requirement of the spatial coherence of the in-line phase contrast imaging, the focal spot size of the x-ray source has to be as small as possible. However, limited focal spot size strongly restricts the tube output power of the x-ray source, thus, limiting the number of output photons in a certain amount of time. The number of x-ray photons N generated from the x-ray focal spot is given as follow [44]:

$$N \propto kVp^2 \cdot mAs \tag{20}$$

where kVp represents the x-ray energy, and mAs represents the tube current in units of milliamperes (mA) multiplied by the exposure time in the unit period (s). From the above formula, one can see that for a given x-ray energy and exposure time, the tube current is limited because of the limited output power. If we want to keep the same amount of output photons, either the exposure time or the x-ray energy should be increased. If we want to increase the exposure time, it has to be increased by the same proportion as the tube current is decreased. Also, the duration of the exposure time in real clinical applications is limited. However, increasing the x-ray energy only requires increasing the square root of this proportion and it is more feasible in the clinical applications. Therefore, the in-line phase contrast imaging using the high-energy x-ray photons has the potential to generate the same amount of x-ray photons in a certain exposure time in order to meet the current clinical requirement. In this study, the high-energy in-line phase contrast prototype system is used to detect the lesion-like objects in breast phantoms.

Chapter 4. Imaging Systems

4.1 X-ray Imaging Systems

4.1.1 Geometry of X-ray Imaging Systems

A unique in-line phase contrast imaging test bed has been developed and assembled in our research laboratory. The basic structure of the test bed is presented and discussed as following. The geometry of the high-energy in-line phase contrast imaging prototype system is shown in Figure 4-1 (a) and the geometry of the conventional x-ray imaging system is shown in Figure 4-1 (b). In the high-energy in-line phase contrast imaging for the 50G/50A breast phantom, the source-to-object distance (SOD, R1) is 68.58 cm and the source-to-image distance (SID, R1+R2) is 137.16 cm, given the geometric magnification factor M of 2. For the 70G-30A breast phantoms, the SOD is 68.58 cm and the SID is 168.9 cm, with the magnification factor of 2.46. In order to keep the same entrance radiation dose level, the SOD of the conventional x-ray imaging is same as the SOD of the high-energy in-line phase contrast x-ray prototype system. Also, in the conventional x-ray imaging, there is no air gap between the object and the detector.

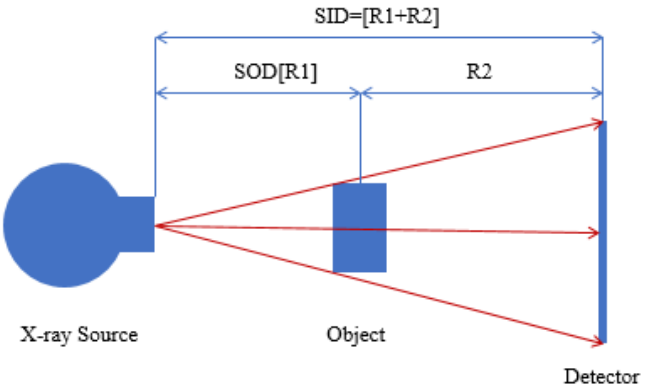

(a)

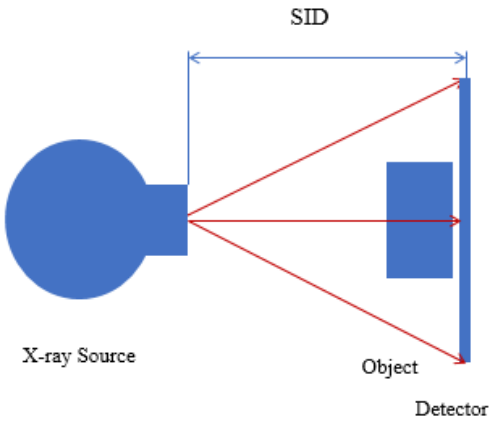

(b)

Figure 4-1: X-ray imaging systems: (a) high-energy in-line phase contrast prototype system (b) conventional x-ray system

4.1.2 Microfocus X-ray Source

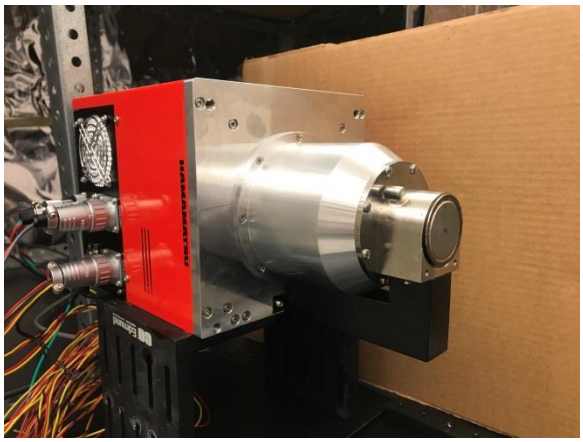

Figure 4-2: Micro-focus x-ray source

As shown in Figure 4-2, a micro-focus x-ray source (Model L9181-06, Hamamatsu Photonics, Japan) is utilized in this study. The tube operates in two modes, continuous emission and pulse emission modes. This x-ray tube has a tungsten (W) target and a Beryllium (Be) output window with the thickness of 500 μm. The distance between the focal spot to the output window is 13 mm and the x-ray beam angle is approximately 100 degree. The tube voltage and tube current are adjustable, with the range of 40-130 kVp and 10-300 μA, respectively. The output power of the x-ray tube is determined by:

$$Power\ (W) = IV$$

where I represents the tube current and the V represents the tube voltage. The x-ray source has a varying focal spot size ranging from 16-50 μm depending on its output power. The relationship between the output power and focal spot size is determined by the formula given by its manufacturer [60]:

$$Focal\ spot\ size\ (\mu m) = 0.999 * \mathrm{P\ (W)} + 10.27 \quad (21)$$

The complete details of the x-ray tube and its characterizations can be found in ref [60]. In this study, the operating settings of the tube results in a focal spot size of 22.3 μm in conventional imaging while the operating settings of the tube results in 18.3 μm for the high-energy in-line phase contrast prototype system.

4.1.3 Beam Hardening

Owing to the fact that the x-ray source applied in the clinical application is a polychromatic x-ray source, there will be a great amount of low energy x-ray photons emitted from the x-ray source. However, the penetration ability of the low energy x-ray photons is very low, which means these photons will be simply absorbed by human body and will result in no contribution to the image signals. Low energy x-ray photons are harmful to patients because they can increase the meaningless radiation dose. Thus, in real applications, x-ray filters are applied in order to block the low x-ray energy photons. In this study, we applied a 2.0 mm thick aluminum (Al) filter for the high-energy in-line phase contrast imaging prototype system and a 0.05 mm thick rhodium (Rh) filter for the conventional x-ray system.

4.1.4 Detector System

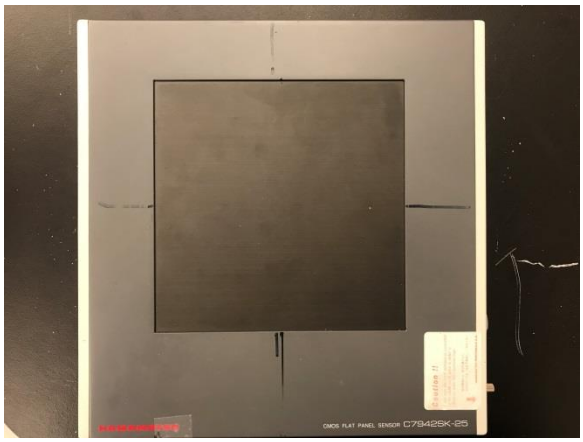

Figure 4-3: CMOS flat panel detector

As shown in Figure 4-3, a CMOS flat panel detector (C7942SK-25, Hamamatsu Photonics, Japan) is used for imaging in this study. It has a photosensitive area of 120 x 120 mm with a pixel array of 2316×2316. The detector has a pixel size of 50 µm x 50 µm. A Cesium Iodide (CSI) intensifying screen used to for the conversion of the incident x-ray beams to visible light photons.

4.2 Ultrasound Imaging Systems

Two ultrasound systems are used in this study. One is the Acuson X300 Ultrasound System, Premium Edition (Siemens Medical Solutions, Malvern, PA). This ultrasound system is equipped with two transducers: the first one is the VF13-5 transducer (Siemens Medical Solutions, Malvern, PA), which generates the ultrasound wave with the resonant frequency of 11.4 MHz. The second transducer is the C7F2-4D transducer (Siemens Medical Solutions, Malvern, PA), which generates the ultrasound wave with the resonant frequency of 5.0 MHz. The C7F2-4D transducer was placed on the phantom and swiped across the phantom to scan the embedded carbon fiber disks and reconstruct the 3-D ultrasonic image. This

detection is done in the College of Allied Health (University of Oklahoma, Oklahoma City, Oklahoma). The other ultrasound system is the Ultrasonix SonixOne® (Ultrasonix, Richmond, BC, Canada), as shown in Figure 3-4. This ultrasound system is equipped with two transducers: the L40-8/12 (Ultrasonix, Richmond, BC, Canada) and 4DL14-5 (Ultrasonix, Richmond, BC, Canada). The L40-8/12 transducer has the frequency range of about 40-8 MHz and the image field of 16 mm. The 4DL14-5 has the frequency range of about 14-5 MHz and the image field of 28 mm. The 4DL14-5 transducer is used to detect the objects inside the breast phantoms with the resonant frequency of 6.6 MHz.

Figure 4-4: Ultrasonix SonixOne® ultrasound system

Chapter 5. Multipurpose Breast Phantoms

In preclinical mammography studies, breast phantoms are routinely employed in the performance evaluation of the developed imaging prototype systems [61-63]. A multipurpose breast phantom can mimic real breast tissues under particular conditions when it is imaged by different imaging modalities, for example, the mammography, the ultrasound, and the computed tomography (CT). The requirement of multipurpose breast phantom used in this study should not only be able to mimic the high-density breasts (breast glandular proportion greater than 50% [64]) under the x-ray imaging but also can be applied in ultrasound imaging. Unfortunately, to the best of our knowledge, there is no high-density multiply-purpose breast phantom available in the market because it has not currently been certified to be commercialized by the FDA (Food & Drug Administration). Some other breast phantoms, for example, the solid breast tissue equivalent phantoms, can mimic the high-density breast under single imaging equipment, but they cannot be utilized in both ultrasound imaging and x-ray imaging. Thus, in order to compare the performance of high-energy in-line phase contrast imaging with the traditional method in breast cancer detection, we used a lab-made glandularity-adjustable dual-purpose breast tissue equivalent phantom developed by Wu [63]. The composition of the glandularity-adjustable dual-purpose breast tissue equivalent phantom is adjusted to mimic the physical density equals to 70-30 glandular-adipose ratio (70G-30A) breast tissue in this study.

In this thesis, three multipurpose breast phantoms are employed to evaluate the performance of the high-energy in-line phase contrast imaging: a commercialized 50% glandular and 50% adipose (50G-50A) multipurpose breast phantom and two 70G-30A

lab-made breast phantoms embedded with carbon fibers disks and gelatin blocks, respectively. The method of developing the glandularity-adjustable dual-purpose breast tissue equivalent phantom and the introduction of each phantoms is given in this chapter.

5.1 50G-50A Multipurpose Breast Phantom

A breast-shaped phantom (Model 073, Computerized Imaging Reference Systems, Virginia, USA) is used to mimic the 50G-50A heterogeneous appearance breast tissue under ultrasound and x-ray imaging. The background of the phantom is made by Zerdine® gel (US PATENT# 5196343) developed by CIRS company. The Zerdine® gel is mainly made of solid-elastic polymer with a water-based property. The Z-Skin™ membrane (CIRS, USA) material is used to simulate the shape and the feeling of the skin during the ultrasound scanning. About 5-10 cystic masses and 10-15 dense masses are embedded within the breast phantom. The cystic masses with spherical or elliptical shape consists of water and thickening agent. The dense masses are made of the Zerdine®-based material with spiculated shape [65]. The dimensions of the phantom are 12 cm × 10 cm × 9 cm.

The phantom is imaged by the high-energy in-line phase contrast prototype system under the conditions of 120 kVp, 67 μA tube current, and 4.4 seconds exposure time and it is also imaged by the conventional x-ray system under the conditions of 40 kVp, 300 μA tube current, and 11 seconds exposure time. The radiation dose for both high-energy in-line phase contrast imaging and conventional imaging is 0.12 mGy.

5.2 70G-30A Multipurpose Breast Phantoms

As mentioned previously, owing to the fact there is no commercial multipurpose high-density breast phantom available in the market, laboratory-made glandularity-adjustable dual-purpose breast tissue equivalent phantoms are employed to mimic the high-density breast tissue in this study. The composition of this phantom consists of water, gelatin with the bloom rate of 300 from porcine skin (Sigma Aldrich®), dextrin fiber (Equate™), Intralipid 20% emulsion (Phospholipid stabilized soybean, Sigma Aldrich®), Glycerol ACS reagent ≥ 99.5% (Sigma Aldrich®) and Soybean oil. These ingredients are used to make the background object of the normal high-density breast tissue as well as the gelatin blocks with the glandular ratio of 80% and 85%, respectively. The gelatin blocks are embedded into the breast phantoms to mimic the breast lesions. The proportion of each component to make the breast phantoms and the gelatin blocks with different glandular proportions is shown in table 5-1:

Table 5-1: Composition of various compounds for the glandularity-adjustable dual-purpose breast eissue equivalent phantom with different glandular ratios

Glandular Ratio / Components (g)	70%	80%	85%
Water (H_2O)	67	70	76
Gelatin ($C_6H_{12}O_6$)	5.6	6	6.8
Fiber ($C_6H_{12}O_5$)	25	3.92	4.06
Phospholipid	3.9	5.67	6.4
Glycerol ($C_3H_3O_3$)	5.3	26.8	30.4
Soybean Oil	33.8	28.2	16.9

Detailed introduction of the development and the equivalency validations of the glandularity-adjustable dual-purpose breast tissue equivalent phantoms is given in ref. [66].

Figure 5-1: 70G-30A breast phantom embedded with gelatin blocks

In this study, two 70G-30A breast phantoms made with same ingredient and shape but embedded with different lesion-like objects are employed in this study. The thickness of the two breast phantoms are 5 cm. The first phantom (Phantom 70G-30A-1) is embedded with eight carbon fiber disks. These circular disks has multiple diameters and thicknesses range from 6 mm to 11.6 mm and 0.4 mm to 1.7 mm, respectively.

As shown in Figure 5-1, the second breast phantom (Phantom 70G-30A-2) is embedded with gelatin blocks. Five gelatin blocks at the first column mimics the 80G-20A glandular/adipose composition breast tissue while the other five gelatin blocks at the second column mimics the 85G-15A glandular/adipose composition breast tissue are embedded in this breast phantom. The thicknesses of the gelatin blocks varies from 0.8 mm to 10.3 mm at each column.

Both phantoms are exposed by the high-energy in-line phase contrast prototype system under the conditions of 120 kVp, 67 μA tube current, 18 seconds exposure time and also exposed by the conventional x-ray system under the conditions of 40 kVp, 300 μA tube current, 50 seconds exposure time. The glandular dose for both high-energy in-line phase contrast imaging and conventional imaging is 0.60 mGy.

Chapter 6. Performance Evaluation of the High-energy In-line Phase Contrast Imaging

6.1 50G-50A Breast Phantom

As detailed in Chapter 4, the images of 50G-50A multipurpose breast phantom are acquired by the conventional x-ray imaging, the high-energy in-line phase contrast prototype system and the ultrasound imaging system, respectively. The imaging settings for the conventional and the high-energy in-line phase contrast prototype system are given in Table 6-1. Since there is no air gap between the object and the detector, the magnification factor (M) in conventional x-ray imaging is 1. The Ultrasonix SonixOne® Ultrasound Imaging System is used to generate the ultrasound images for the phantoms.

Table 6-1: X-Ray imaging settings

Imaging Conditions	Phase Contrast Prototype	Conventional X-ray
Tube Voltage	120 kVp	40 kVp
Tube Current	67 µA	300 µA
Exposure Time	4.4 s	11s
SOD	68.58 cm	68.58 cm
SID	137.16 cm	68.58 cm
Magnification Factor	2	1
Focal Spot Size	18.3 µm	22.3 µm

The images acquired by the ultrasound imaging system are shown in Figure 6-1 and the conventional x-ray image and the high-energy in-line phase contrast image are shown in Figure 6-2.

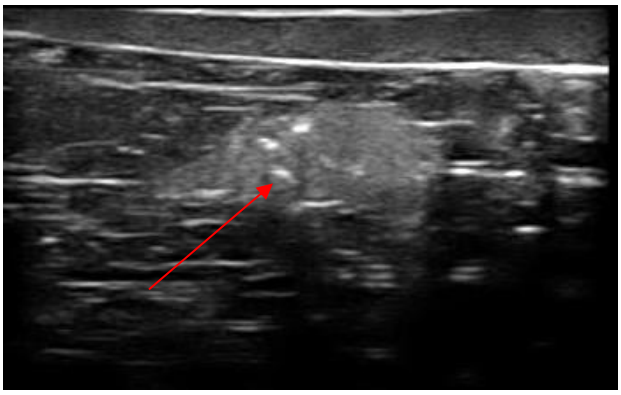

(a)

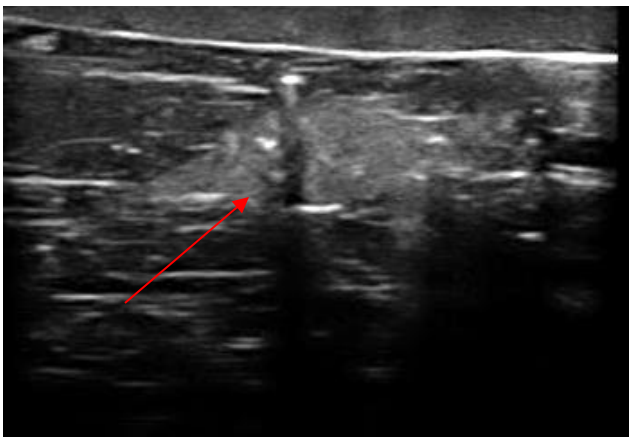

(b)

Figure 6-1: Ultrasound images of 50G-50A breast phantom (a) without needle inserted (b) with needle inserted

In order to demonstrate that the lesion-like object found by the x-ray imaging systems is exactly the one detected by the ultrasound system, a metal needle is inserted in the breast phantom as a marker. One can easily find that the lesion-like object embedded in the breast phantom can be detected by the ultrasound images.

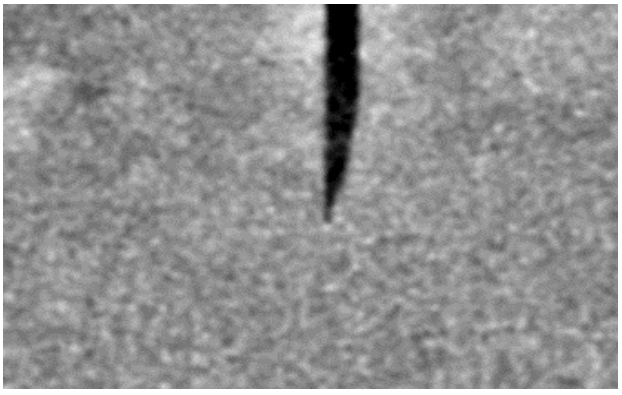

(a)

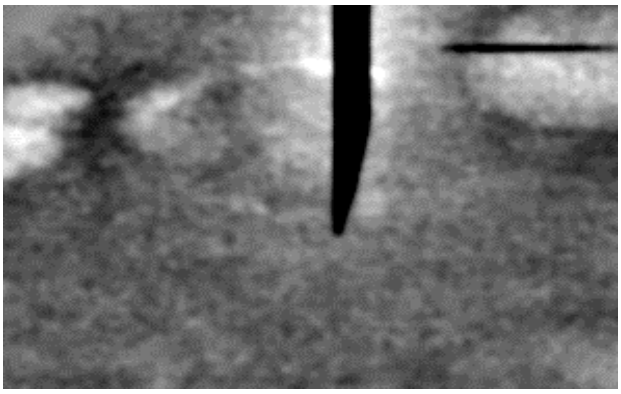

(b)

Figure 6-2: 50G-50A breast phantom imaged by the (a) conventional x-ray imaging system (b) high-energy in-line phase contrast prototype system

The breast phantom images acquired by the two x-ray imaging systems are shown in Figure 6-2. As shown in the figure, the location of the embedded object is hard to detect from image acquired by the conventional x-ray imaging system (Figure 6-2(a)). The tumor like pattern can be clearly detected from the image acquired by the high-energy in-line phase contrast x-ray prototype (Figure 6-2 (b)).

6.2 70G-30A Breast Phantoms

In the imaging of 70G-30A breast phantoms, all the acquisition parameters for both the x-ray imaging systems are same as the settings in the 50G-50A breast phantom except the SID and exposure time. The SID is changed to 168.91 cm, resulting in a magnification factor (M) of 2.46 in the high-energy in-line phase contrast x-ray imaging. The exposure time is changed to 18 seconds for the high-energy in-line phase contrast imaging and 50 seconds for the conventional x-ray imaging. The dose levels for conventional and phase contrast imaging for these phantoms are 0.60 mGy. The Acuson X300 Ultrasound System

and the Ultrasonix SonixOne® Ultrasound System is used to acquire the images of the breast phantom embedded with carbon fiber disks and breast phantom embedded with gelatin blocks.

6.2.1 Acquired Images

6.2.1.1 70G-30A Breast Phantom Embedded with Carbon Fiber Disks

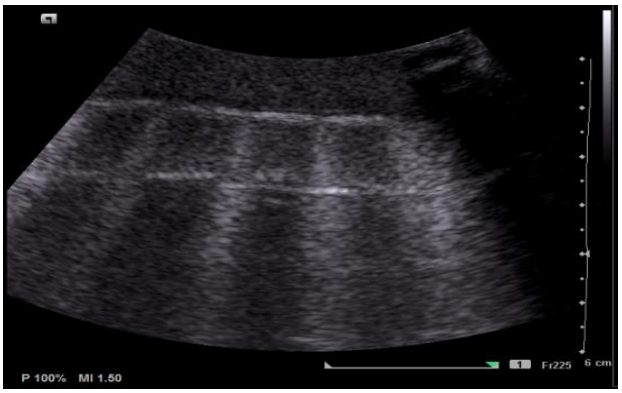

(a)

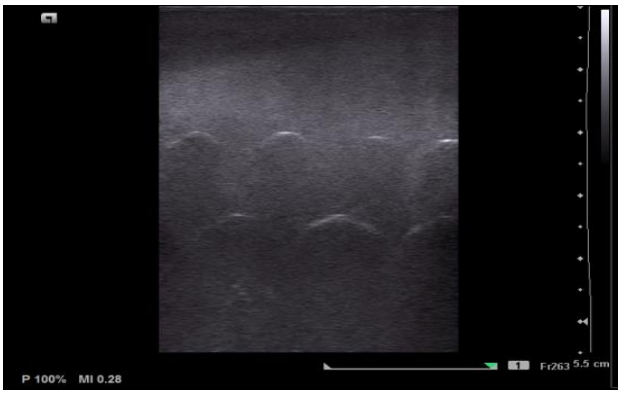

(b)

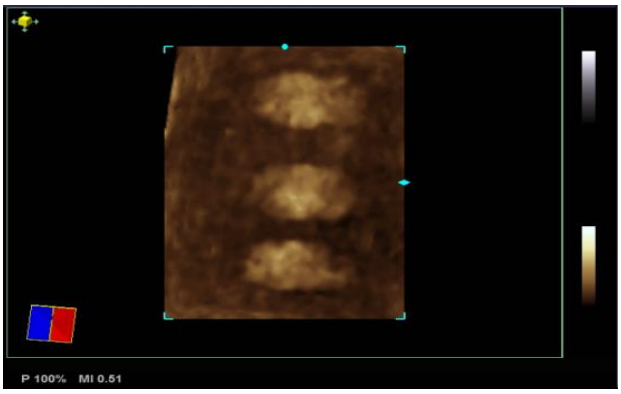

(c)

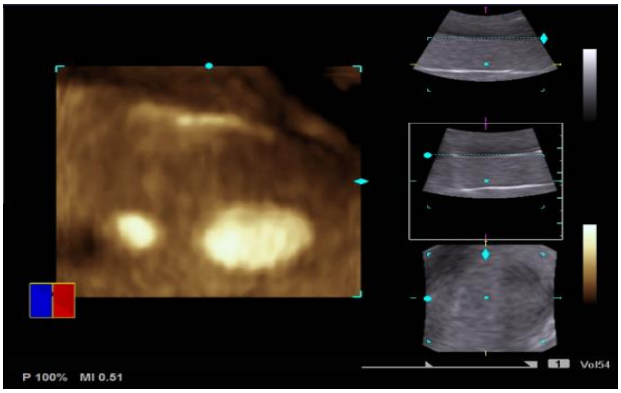

(d)

Figure 6-3: Ultrasound images of 70G-30A breast phantom embedded with carbon fiber disks

The ultrasound images detected by Ultrasonix SonixOne® Ultrasound System are provided in Figure 6-3((a)-(b)). Figure 6-3(a) demonstrates the image detected in the coronal plane and Figure 6-3 (b) demonstrates the image detected in the sagittal plane. All the carbon fiber disks are able to be detected by Ultrasonix SonixOne® Ultrasound System, however the full circular boundaries of the carbon fiber disks can't be detected by this system. Figure 6-3(c)-(d) is the 3-D ultrasound images generated by Acuson X300 Ultrasound System. Figure 6-3(c) demonstrates the three smallest carbon fiber disks in the breast phantom and while

6-3(d) demonstrates the biggest (on the right) and smallest (on the left) of the carbon fiber disks. All the carbon fiber disks can be detected by this imaging system. Also, the complete circular boundaries of the carbon fiber disks can be detected by this imaging system.

(a)

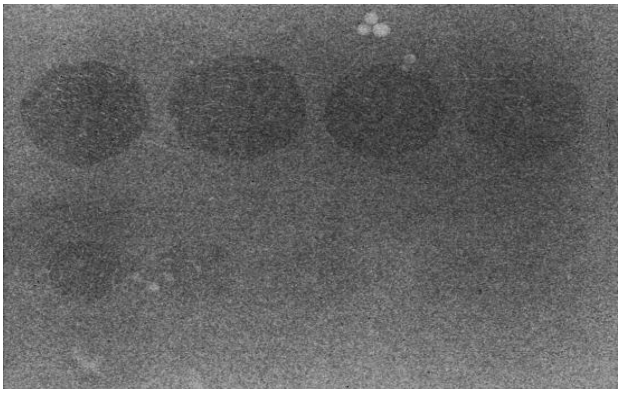

(b)

Figure 6-4: 70G-30A breast phantom embedded with carbon fiber disks imaged by (a) conventional x-ray imaging system (b) high-energy in-line phase contrast prototype system

Figure 6-4 demonstrates the acquired image by the conventional x-ray imaging (6-4(a)) and the high-energy in-line phase contrast imaging (6-4(b)), respectively. One can see that

it is hard to visually detect the location and the boundary of the carbon fiber disks in the conventional x-ray image. But some of the disks are clearly detectable by the high-energy in-line phase contrast imaging. As the thickness and the diameters of the carbon fiber disks are getting smaller, the detectability of the disks decrease in the the high-energy in-line phase contrast imaging.

6.2.1.2 70G-30A Breast Phantom Embedded with Gelatin Blocks

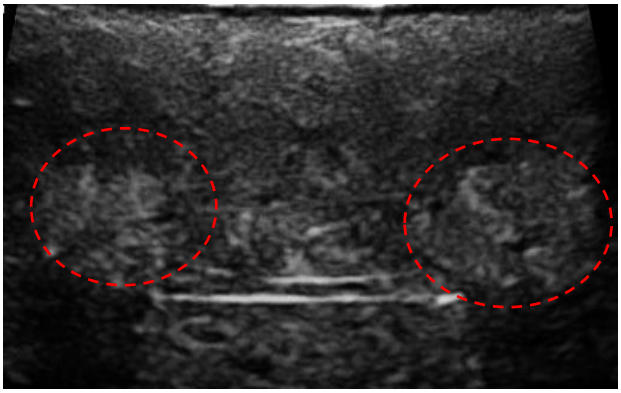

(a)

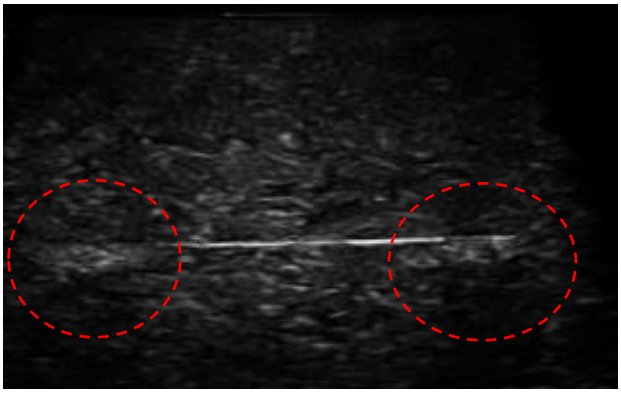

(b)

Figure 6-5: Ultrasound images of 70G-30A breast phantom embedded with gelatin blocks

In the detection of 70G-30A breast phantom embedded with gelatin blocks, all the gelatin blocks can be detected by the Ultrasonix SonixOne® ultrasound system. Figure 6-5 shows the biggest gelatin blocks (Figure 6-5(a)) and the smallest gelatin blocks (Figure 6-5 (b)) with the glandular proportions of 80% and 85%. These figures show that the ultrasound imaging can clearly reveal the locations of the gelatin blocks and the detectability for the gelatin blocks with different glandular density is almost same.

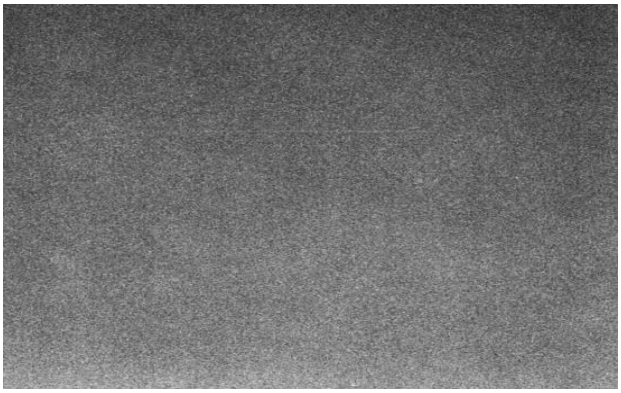

(a)

(b)

Figure 6-6: 70G-30A breast phantom embedded with carbon fiber disks imaged by (a) conventional x-ray imaging system (b) high-energy in-line phase contrast prototype system

Figure 6-6 demonstrates the acquired images of the 70G-30A breast phantom embedded with gelatin blocks by the conventional x-ray imaging (Figure 6-6(a)) and the high-energy in-line phase contrast image (Figure 6-6(b)). The figure reveals that it is still hardly to visually detect any gelatin blocks on the conventional x-ray images. But, some of the gelatin blocks can be detected by using the high-energy in-line phase contrast imaging prototype system. In addition, since the glandular density of the 80% gelatin blocks is closer to the glandular density of the phantom background, the contrast seems to be smaller compared with the 85% glandular density gelatin blocks. Furthermore, as the thickness of the gelatin blocks is getting smaller, some of the gelatin blocks are still hard to be found by the high-energy in-line phase contrast x-ray imaging.

6.2.2 Observer Performance Studies

Observer performance study is a subjective approach to provide qualitative analysis on the image in order to evaluate the performance of the image modalities. The results of the observe study is determined by the observer's ability to distinguish the objects from the background. Currently, the observer study has been applied in different breast phantoms, for example, the contrast detail phantom, the CDMAM phantom and the ACR phantom. In order to more accurately evaluate the performance of the high-energy in-line phase contrast imaging prototype in the detection of human breast, the observer study for x-ray images of the 70G-30A breast phantoms are performed in this study.

Nine observers are engaged in this observer study. The observers are asked to distinguish the outline of the objects in the images using Image J software and provide a score to indicate the degree of discernibility of an object. The observers can adjust the window

leveling settings, contrast and image magnification in order to suit their visual preferences. The x-ray images of 70G-30A breast phantoms are presented to the observers and the observers completed all of the studies independently. For the 70G/30A breast phantom embedded with carbon fiber disks, the scoring methods is as follows: First, if the full circle of the disks are visible, it is scored as 1 point. Second, if the full circle is not able to be distinguished but half or more than half of the circle is distinguishable, it is scored as 0.5 point. Third, if less than half circle or no object is distinguishable, it is scored as 0 point. For the 70G-30A breast phantom embedded with gelatin blocks, the scoring methods is as follows: First, if the total number of four sides of the squares can be identified, it is scored as 1 point. Second, if the observers cannot distinguish all the four sides but two and more than two sides are identified, it is scored as 0.5 point. Third, if only one or none of the sides are identified, it is scored as 0 point. The observers can analyze the images on the screen and use the paintbrush tool to mark and score the objects. The analysis results of each observer would then be averaged for each image and be demonstrated on a graph. The detailed descriptions of the 70G-30A breast phantoms and each embedded objects is given shown in Section 5.2. The study is done on a TFT LCD monitor with Max Preset Resolution of 1920 x 1080 at 60 Hz, Contrast Ratio of 1000:1 and Pixel Pitch of 0.265 mm in the same viewing conditions.

In order to determine the most suitable statistical analysis approach in the observer study, two situations should be taken into account: First, the size of the samples used in this study is only nine, which is extremely small for a statistical standpoint. Second, the variance of the data in this study is unknown. Based on the two factors, the student t distribution is

used as the optimal statistical method for the data analysis. The standard deviation S of the sample is given by the following equation:

$$S = \sqrt{\frac{\sum_{i=1}^{n}(Y_i - \bar{Y})^2}{n-1}} \tag{22}$$

where n is the total number of the observers engaged in this study, Y_i is the point value given by Observer i and $\bar{Y}$ is the averaged point value from averaging all the observers' analysis. A 95% confidence interval with the degree freedom of n-1 is applied in the statistical analysis, given the corresponding interval:

$$\bar{Y} \pm t_{\frac{\alpha}{2},n-1}\frac{S}{\sqrt{n}} \tag{23}$$

where n (n=9) is the total number of the observers engaged in this study, $\bar{Y}$ is the averaged point value from scored by all the obverses, S is the variance of the score and $t_{\frac{\alpha}{2},n-1}$ is the Student t value corresponding to 95% confidence with n-1 degree of freedom.

6.2.2.1 Observer study of 70G-30A Breast Phantom Embedded with Carbon Fiber Disks

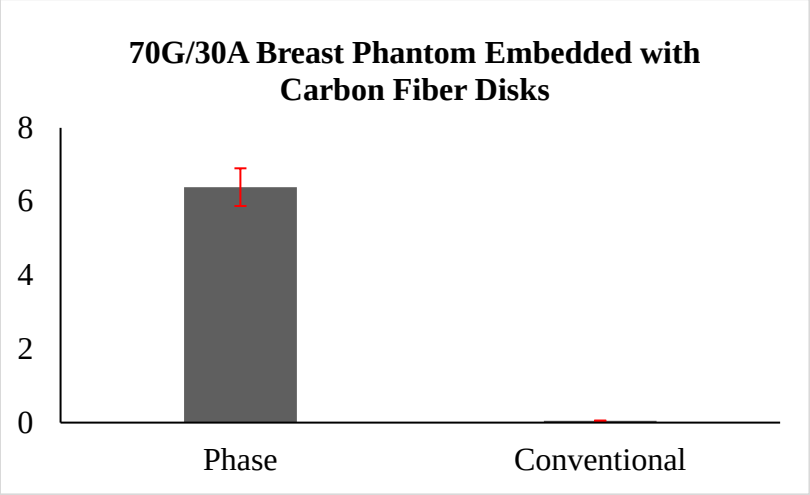

Figure 6-7: Observer performance study of the 70G-30A breast phantom embedded with carbon fiber disks

The result of the observer study of 70G-30A breast phantom embedded with carbon fiber disks is demonstrated in Figure 6-7. It shows that none of the disks are visually found by the observers from the conventional x-ray imaging but some of the carbon fiber disks (6.39 ± 0.57) are detected by the observers.

6.2.2.2 Observer Study of 70G-30A Breast Phantom Embedded with Gelatin Blocks

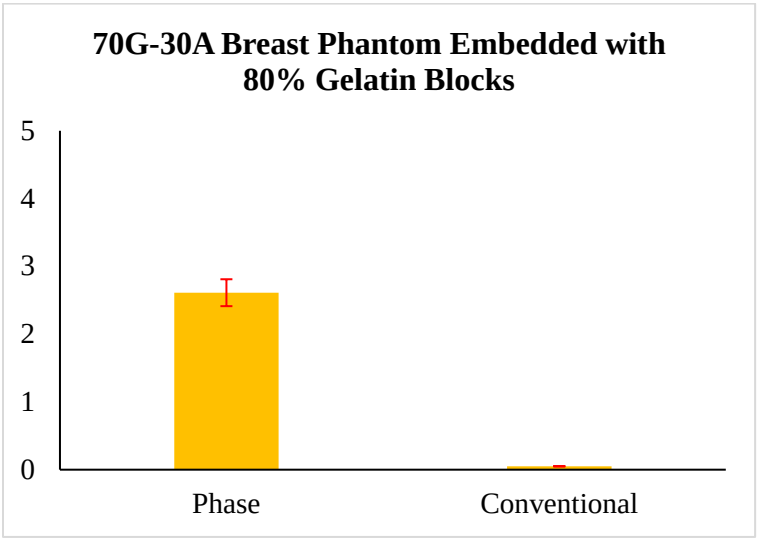

(a)

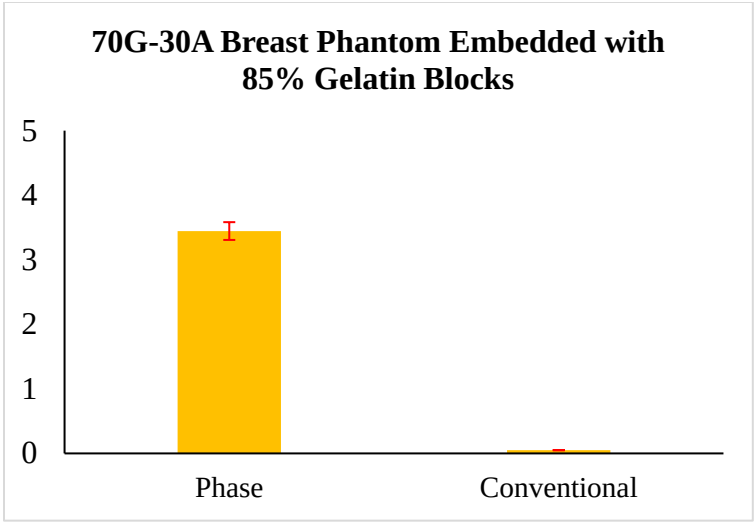

(b)

Figure 6-8: Observer performance study of the 70G-30A breast phantom embedded with gelatin blocks with the glandular proportion of (a) 80% and (b) 85%

The results of the observer study of 70G-30A breast phantom embedded with gelatin blocks are demonstrated in Figure 6-8. None of the embedded lesion-like objects in the

conventional x-ray images are found by the observers. In the high-energy in-line phase contrast imaging, several but not all of the gelatin blocks can be found by the observer. Also, the observers can found more gelatin blocks with the 85% glandular proportion (3.44 ± 0.12) compared with 80% glandular proportion gelatins blocks (2.61 ± 0.17). This is within our expectation because the 80% glandular gelatin blocks has smaller density difference with the background materials. This may cause less phase shift differences when the x-ray passing through the 80% glandular density gelatin blocks and the breast phantom background. The smaller phase shift difference will then contribute to smaller contrast generated by the phase contrast effect.

Chapter 7. Discussion and Conclusion

7.1 Study summary

The primary objective of the research presented in this thesis is to demonstrate the potential of applying the high-energy in-line phase contrast prototype system in the detection of the breast tumor in dense breasts. This study compared the performance of the high-energy in-line phase contrast imaging with the performance of the traditional x-ray imaging modality and ultrasound imaging. Three breast phantoms are used as the imaging objects in this study: a 50G/50A breast phantom and two 70G/30A breast phantoms embedded with carbon fiber disks and gelatin blocks, respectively. The observer study is applied to analyze the performance of the x-ray imaging modalities. As the results, the high-energy in-line phase contrast prototype system shows a better performance compared with the conventional x-ray imaging. However, some of the lesion-like objects detected by the ultrasound imaging systems are not able to be detected by the high-energy in-line phase contrast prototype system. Thus, there is still a room to improve the performance of this new prototype system in the future.

7.2 Challenges

There are still a number of challenges remained in promoting the high-energy in-line phase contrast imaging prototype system in the clinical breast cancer detection.

Firstly, the 70G/30A breast phantom used in this study mimics homogeneous background of the breast tissue with the average physical density equals to 70% glandular/30% adipose. However, in the real anatomy of the human breast, the glandular tissue is randomly

distributed in the human breast. Thus, the background of human breast should be heterogeneous instead of homogeneous. Therefore, this applied 70G/30A breast phantom simplified the real structure and cannot exactly present the real human breast in clinical application. Thus, a more dedicated breast phantom need to be developed to mimic the real human breast conditions in the future.

Secondly, the breast phantom employed in this study is a self-made phantom in the lab. Even though this method is a direct and convenient design for this study, it may still have some imperfection: 1. Since it is a self-made breast phantom, it is possible that there might be some deviation in weighing the component of the breast phantom, which lead to the fact that the glandular/adipose composition of the phantom may not be exactly 70G/30A. 2. The phantom is a temporary phantom, which means it cannot last long in the outside environment. The element of the phantom is interacting with the element in the air and the water contained in the phantom may evaporating right after the phantom is made. Thus, it is difficult to keep the phantom the exact component as the 70G/30A breast phantom. Therefore, a more standard 70G/30A breast phantom is still required in the future.

Lastly, from the prototype component used in this study, the focal spot size of the x-ray source needs to be as small as possible in order to maintain the necessary of spatial coherence for optimizing the phase contrast effect. However, most commercial micro-focus x-ray source can’t reach enough output power and image the patients in a short time duration. Thus, the third challenges need to overcome is to have a micro-focus x-ray source with higher output power in order to reduce the exposure time.

7.3 Future Research Direction

Further research should firstly focus on overcoming the challenge listed in the previous section. This includes designing breast phantom that is more close to the anatomical structure of the real breast, utilizing a micro-focus x-ray source with enough output power, and decreasing the geometry length of the prototype system. Moreover, further research should also focus on the employment the image objects, such as experimental animals, to make the image condition to be more close to the real clinical applications.

References

1. Siegel, Rebecca L., Kimberly D. Miller, and Ahmedin Jemal. "Cancer statistics, 2017." CA: a cancer journal for clinicians67.1 (2017): 7-30.
2. Nyström, L., et al. "Breast cancer screening with mammography: overview of Swedish randomised trials." The Lancet 341.8851, 973-978 (1993).
3. Friedewald, Sarah M., et al. "Breast cancer screening using tomosynthesis in combination with digital mammography." Jama 311.24, 2499-2507 (2014).
4. US Preventive Services Task Force. "Screening for breast cancer: US Preventive Services Task Force recommendation statement." Annals of internal medicine 151.10, 716 (2009).
5. Auweter, S. D., et al. "X-ray phase-contrast imaging of the breast—advances towards clinical implementation." The British journal of radiology 87.1034, 20130606 (2014).
6. Independent UK Panel on Breast Cancer Screening. "The benefits and harms of breast cancer screening: an independent review." The Lancet 380.9855, 1778-1786 (2012).
7. Smith, Robert A., et al. "Cancer screening in the United States, 2016: A review of current American Cancer Society guidelines and current issues in cancer screening." CA: a cancer journal for clinicians 66.2, 95-114 (2016).
8. Boyd, Norman F., et al. "Mammographic density and the risk and detection of breast cancer." New England Journal of Medicine 356.3, 227-236 (2007).
9. Freimanis, Rita I., and Margaret Yacobozzi. "Breast cancer screening." North Carolina medical journal 75.2, 117-120 (2014).

10. Yaghjyan, Lusine, et al. "Mammographic breast density and subsequent risk of breast cancer in postmenopausal women according to tumor characteristics." Journal of the National Cancer Institute 103.15, 1179-1189 (2011).
11. Rafferty, Elizabeth A., et al. "Breast cancer screening using tomosynthesis and digital mammography in dense and nondense breasts." Jama 315.16, 1784-1786 (2016).
12. Johns, Paul C., and Martin J. Yaffe. "X-ray characterisation of normal and neoplastic breast tissues." Physics in Medicine & Biology 32.6, 675-695 (1987).
13. Sprague, Brian L., et al. "Prevalence of mammographically dense breasts in the United States." JNCI: Journal of the National Cancer Institute 106.10 (2014).
14. Boyd, Norman F., et al. "Mammographic density and the risk and detection of breast cancer." New England Journal of Medicine 356.3, 227-236 (2007).
15. Van Gils, Carla H., et al. "Mammographic breast density and risk of breast cancer: masking bias or causality?." European journal of epidemiology 14.4, 315-320 (1998).
16. Harvey, Jennifer A., and Viktor E. Bovbjerg. "Quantitative assessment of mammographic breast density: relationship with breast cancer risk." Radiology 230.1, 29-41 (2004).
17. Siu, Albert L. "Screening for breast cancer: US Preventive Services Task Force recommendation statement." Annals of internal medicine 164.4, 279-296 (2016).
18. Zanotel, Martina, et al. "Automated breast ultrasound: basic principles and emerging clinical applications." La radiologia medica 123.1, 1-12 (2018).

19. Fitzgerald, Richard. "Phase-sensitive x-ray imaging." Phys. Today 53.7, 23-26 (2000).
20. Matsuo, Satoru, et al. "Evaluation of edge effect due to phase contrast imaging for mammography." Medical physics 32.8, 2690-2697 (2005).
21. Pogany, A., D. Gao, and S. W. Wilkins. "Contrast and resolution in imaging with a microfocus x-ray source." Review of Scientific Instruments 68.7, 2774-2782 (1997).
22. Wilkins, S. W., et al. "Phase-contrast imaging using polychromatic hard X-rays." Nature 384.6607, 335-338 (1996).
23. Wu, Xizeng, and Hong Liu. "Clinical implementation of x-ray phase-contrast imaging: Theoretical foundations and design considerations." Medical physics 30.8, 2169-2179 (2003).
24. Arfelli, F., et al. "Low-dose phase contrast x-ray medical imaging." Physics in Medicine & Biology 43.10, 2845-2852 (1998).
25. Pfeiffer, Franz, et al. "Phase retrieval and differential phase-contrast imaging with low-brilliance X-ray sources." Nature physics 2.4, 258-261 (2006).
26. Kotre, C. J., and I. P. Birch. "Phase contrast enhancement of x-ray mammography: a design study." Physics in Medicine & Biology 44.11, 2853-2866 (1999).
27. Ingal, Viktor N., et al. "Phase mammography-a new technique for breast investigation." Physics in Medicine & Biology 43.9, 2555-2567 (1998).
28. Fedon, Christian, et al. "Dose and diagnostic performance comparison between phase-contrast mammography with synchrotron radiation and digital

mammography: a clinical study report." Journal of Medical Imaging 5.1, 013503 (2018).

29. Ghani, Muhammad U., et al. "Detectability comparison between a high energy x-ray phase sensitive and mammography systems in imaging phantoms with varying glandular-adipose ratios." Physics in Medicine & Biology 62.9 (2017): 3523.
30. Ghani, Muhammad U., et al. "Detectability comparison of simulated objects within a dense breast phantom using high energy x-ray phase sensitive and conventional imaging systems." Biophotonics and Immune Responses XII. Vol. 10065. International Society for Optics and Photonics, 2017.
31. Ghani, Muhammad U., et al. "Low dose high energy x-ray in-line phase sensitive imaging prototype: Investigation of optimal geometric conditions and design parameters." Journal of X-ray science and technology 23.6 (2015): 667-682.
32. Wu, Di, et al. "Phantom study based on a high-energy in-line phase contrast tomosynthesis prototype." SPIE 8944, 89440G (2014).
33. Wu, Di, et al. "Characterization of a high-energy in-line phase contrast tomosynthesis prototype." Medical physics 42.5, 2404-2420 (2015).
34. Wong, Molly Donovan, et al. "Dose and detectability improvements with high energy phase sensitive x-ray imaging in comparison to low energy conventional imaging." Physics in Medicine & Biology 59.9 (2014): N37.
35. Zhang, Da, et al. "In-line Phase-sensitive X-ray Imaging." Advances in Medical Physics, DJ Godfrey, SK Das, and AB Wolbarst, eds.(Medical Physics Publishing, 2014): 143.

36. Ghani, Muhammad U., et al. "Detectability comparison of simulated tumors in digital breast tomosynthesis using high-energy X-ray inline phase sensitive and commercial imaging systems." Physica Medica 47 (2018): 34-41.
37. Wong, Molly, Xizeng Wu, and Hong Liu. "Image quality comparison of high-energy phase contrast x-ray images with low-energy conventional images: phantom studies." SPIE 7563, 756305 (2010).
38. Stampanoni, Marco, et al. "The first analysis and clinical evaluation of native breast tissue using differential phase-contrast mammography." Investigative radiology 46.12, 801-806 (2011).
39. Wong, Molly Donovan, Xizeng Wu, and Hong Liu. "Image quality and dose efficiency of high energy phase sensitive x-ray imaging: Phantom studies." Journal of X-ray Science and Technology 22.3, 321-334 (2014).
40. Ghani, Muhammad U., et al. "Detectability comparison between a high energy x-ray phase sensitive and mammography systems in imaging phantoms with varying glandular-adipose ratios." Physics in Medicine & Biology 62.9, 3523-3538 (2017).
41. Wong, Molly Donovan, et al. "Dose and detectability improvements with high energy phase sensitive x-ray imaging in comparison to low energy conventional imaging." Physics in Medicine & Biology 59.9, N37-N48 (2014).
42. Ghani, Muhammad U., et al. "Quantitative analysis of contrast to noise ratio using a phase contrast x-ray imaging prototype." SPIE 8582, 85820H (2013).
43. Ghani, Muhammad U., et al. "Low dose high energy x-ray in-line phase sensitive imaging prototype: Investigation of optimal geometric conditions and design parameters." Journal of X-ray science and technology 23.6, 667-682 (2015).

44. Bushberg, Jerrold T., and John M. Boone. The essential physics of medical imaging. Lippincott Williams & Wilkins (2011).
45. Kolb, Thomas M., Jacob Lichy, and Jeffrey H. Newhouse. "Comparison of the performance of screening mammography, physical examination, and breast US and evaluation of factors that influence them: an analysis of 27,825 patient evaluations." Radiology 225.1 (2002): 165-175.
46. Duffy, Stephen W., et al. "Mammographic density and breast cancer risk in breast screening assessment cases and women with a family history of breast cancer." European Journal of Cancer 88 (2018): 48-56.
47. Kelly, Kevin M., et al. "Breast cancer detection using automated whole breast ultrasound and mammography in radiographically dense breasts." European radiology 20.3 (2010): 734-742.
48. Benson, S. R. C., et al. "Ultrasound is now better than mammography for the detection of invasive breast cancer." The American journal of surgery 188.4 (2004): 381-385.
49. Berg, Wendie A., et al. "Combined screening with ultrasound and mammography vs mammography alone in women at elevated risk of breast cancer." Jama 299.18 (2008): 2151-2163.
50. Kuhl, Christiane K., et al. "Mammography, breast ultrasound, and magnetic resonance imaging for surveillance of women at high familial risk for breast cancer." Journal of clinical oncology 23.33 (2005): 8469-8476.
51. Chapman, Dean, et al. "Diffraction enhanced x-ray imaging." Physics in Medicine & Biology 42.11 (1997): 2015.

52. David, C., et al. "Fabrication of diffraction gratings for hard X-ray phase contrast imaging." Microelectronic Engineering84.5-8 (2007): 1172-1177.

53. Zanette, I., et al. "Speckle-based x-ray phase-contrast and dark-field imaging with a laboratory source." Physical review letters 112.25 (2014): 253903.

54. Momose, A. "Demonstration of phase-contrast X-ray computed tomography using an X-ray interferometer." Nuclear Instruments and Methods in Physics Research Section A: Accelerators, Spectrometers, Detectors and Associated Equipment 352.3, 622-628 (1995).

55. Chapman, D., et al. "Medical applications of diffraction enhanced imaging." Breast Disease 10.3-4, 197-207 (1998).

56. Wu, Xizeng, and Hong Liu. "Clarification of aspects in in−line phase−sensitive x−ray imaging." Medical Physics 34.2 (2007): 737-743.

57. Veldkamp, Wouter JH, Martin AO Thijssen, and Nico Karssemeijer. "The value of scatter removal by a grid in full field digital mammography." Medical Physics 30.7, 1712-1718 (2003).

58. Freedman, Matthew T., et al. "Phase contrast digital mammography using molybdenum x-ray: clinical implications in detectability improvement." SPIE 5030, 533 (2003).

59. Lewis, R. A. "Medical phase contrast x-ray imaging: current status and future prospects." Physics in medicine & biology 49.16, 3573-3583 (2004).

60. Ghani, Muhammad U., et al. "Characterization of continuous and pulsed emission modes of a hybrid micro focus x-ray source for medical imaging applications."

Nuclear Instruments and Methods in Physics Research Section A: Accelerators, Spectrometers, Detectors and Associated Equipment 853, 70-77 (2017).

61. Wu, Di, et al. "A method of measuring gold nanoparticle concentrations by x-ray fluorescence for biomedical applications." Medical physics 40.5, 051901 (2013).
62. Wu, Di, et al. "Using microbubble as contrast agent for high-energy x-ray in-line phase contrast imaging: demonstration and comparison study." IEEE Transactions on Biomedical Engineering (2017).
63. Wu, Di, et al. "Quantitative investigation of the edge enhancement in in-line phase contrast projections and tomosynthesis provided by distributing microbubbles on the interface between two tissues: a phantom study." Physics in Medicine & Biology 62.24, 9357-9376 (2017).
64. Carney, Patricia A., et al. "Individual and combined effects of age, breast density, and hormone replacement therapy use on the accuracy of screening mammography." Annals of internal medicine 138.3, 168-175 (2003).
65. http://www.cirsinc.com/file/Products/073/073%20DS%20110617(3).pdf
66. Wu, Di, et al. "Laboratory designs and validations of a glandularity-adjustable dual-purpose breast tissue phantom." SPIE 10573, 105735H (2018).